



HAL
open science

Simultaneous Optical and Electrical Characterization of GaN Nanowire Arrays by Means of Vis-IR Spectroscopic Ellipsometry

Antonio Santos, Bertrand Lacroix, Eduardo Blanco, S. Hurand, Víctor Gómez, Fabien Paumier, Thierry Girardeau, Diana Huffaker, Rafael Garcia, Francisco Morales

► **To cite this version:**

Antonio Santos, Bertrand Lacroix, Eduardo Blanco, S. Hurand, Víctor Gómez, et al.. Simultaneous Optical and Electrical Characterization of GaN Nanowire Arrays by Means of Vis-IR Spectroscopic Ellipsometry. *Journal of Physical Chemistry C*, 2019, 124 (2), pp.1535-1543. 10.1021/acs.jpcc.9b10556 . hal-02464507

HAL Id: hal-02464507

<https://hal.science/hal-02464507v1>

Submitted on 22 Sep 2024

HAL is a multi-disciplinary open access archive for the deposit and dissemination of scientific research documents, whether they are published or not. The documents may come from teaching and research institutions in France or abroad, or from public or private research centers.

L'archive ouverte pluridisciplinaire **HAL**, est destinée au dépôt et à la diffusion de documents scientifiques de niveau recherche, publiés ou non, émanant des établissements d'enseignement et de recherche français ou étrangers, des laboratoires publics ou privés.

This is an Open Access document downloaded from ORCA, Cardiff University's institutional repository: <https://orca.cardiff.ac.uk/id/eprint/129573/>

This is the author's version of a work that was submitted to / accepted for publication.

Citation for final published version:

Santos, Antonio J., Lacroix, Bertrand, Blanco, Eduardo, Hurand, Simon, Gomez, Victor J., Paumier, Fabien, Girardeau, Thierry, Huffaker, Diana L. , García, Rafael and Morales, Francisco M. 2020. Simultaneous optical and electrical characterization of GaN nanowire arrays by means of Vis-IR spectroscopic ellipsometry. *Journal of Physical Chemistry C* 124 (2) , pp. 1535-1543. 10.1021/acs.jpcc.9b10556

Publishers page: <http://dx.doi.org/10.1021/acs.jpcc.9b10556>

Please note:

Changes made as a result of publishing processes such as copy-editing, formatting and page numbers may not be reflected in this version. For the definitive version of this publication, please refer to the published source. You are advised to consult the publisher's version if you wish to cite this paper.

This version is being made available in accordance with publisher policies. See <http://orca.cf.ac.uk/policies.html> for usage policies. Copyright and moral rights for publications made available in ORCA are retained by the copyright holders.



Simultaneous Optical and Electrical Characterization of GaN Nanowire Arrays by Means of Vis-IR Spectroscopic Ellipsometry

Antonio J. Santos, Bertrand Lacroix, Eduardo Blanco, Simon Hurand, Víctor J. Gómez, Fabien Paumier, Thierry Girardeau, Diana L. Huffaker, Rafael Garcia, and Francisco M. Morales

J. Phys. Chem. C, **Just Accepted Manuscript** • DOI: 10.1021/acs.jpcc.9b10556 • Publication Date (Web): 27 Dec 2019

Downloaded from pubs.acs.org on January 1, 2020

Just Accepted

“Just Accepted” manuscripts have been peer-reviewed and accepted for publication. They are posted online prior to technical editing, formatting for publication and author proofing. The American Chemical Society provides “Just Accepted” as a service to the research community to expedite the dissemination of scientific material as soon as possible after acceptance. “Just Accepted” manuscripts appear in full in PDF format accompanied by an HTML abstract. “Just Accepted” manuscripts have been fully peer reviewed, but should not be considered the official version of record. They are citable by the Digital Object Identifier (DOI®). “Just Accepted” is an optional service offered to authors. Therefore, the “Just Accepted” Web site may not include all articles that will be published in the journal. After a manuscript is technically edited and formatted, it will be removed from the “Just Accepted” Web site and published as an ASAP article. Note that technical editing may introduce minor changes to the manuscript text and/or graphics which could affect content, and all legal disclaimers and ethical guidelines that apply to the journal pertain. ACS cannot be held responsible for errors or consequences arising from the use of information contained in these “Just Accepted” manuscripts.

1
2
3
4
5 Simultaneous Optical and Electrical Characterization
6
7
8
9 of GaN Nanowire Arrays by Means of Vis-IR
10
11
12
13 Spectroscopic Ellipsometry
14
15
16
17
18

19 *Antonio J. Santos*^{1,2}, *Bertrand Lacroix*^{1,2}, *Eduardo Blanco*^{2,3}, *Simon Hurand*⁴, *Víctor J.*

20
21
22 *Gómez*^{5 †}, *Fabien Paumier*⁴, *Thierry Girardeau*⁴, *Diana L. Huffaker*^{5,6}, *Rafael García*^{1,2}

23
24
25
26 *and Francisco M. Morales*^{1,2,*}
27
28
29

30
31 ¹ Department of Materials Science and Metallurgic Engineering, and Inorganic

32
33
34 Chemistry, Faculty of Sciences, University of Cádiz, Spain.
35
36
37

38
39 ² IMEYMAT: Institute of Research on Electron Microscopy and Materials of the

40
41
42 University of Cádiz, Spain.
43
44
45

46
47 ³ Department of Condensed Matter Physics, Faculty of Sciences, University of Cádiz,

48
49
50 11510 Puerto Real, Cádiz, Spain.
51
52
53
54
55
56
57
58
59
60

1
2
3
4 ⁴ Institut Pprime, UPR 3346 CNRS-Université de Poitiers-ENSMA, SP2MI, 86962

5
6
7 Futuroscope-Chasseneuil cedex, France.

8
9
10
11 ⁵ School of Engineering, Cardiff University, CF24 3AA, Cardiff, United Kingdom

12
13
14
15
16 ⁶ School of Physics and Astronomy, Cardiff University, CF24 3AA, Cardiff, United

17
18
19 Kingdom

20
21
22
23
24 * Corresponding author: fmiguel.morales@uca.es

25
26
27
28 **ABSTRACT**

29
30
31
32
33
34 We report an original and straightforward method for both optical and electrical
35
36
37 characterization of vertical GaN nanowire arrays epitaxially grown on silicon through
38
39
40 visible-infrared spectroscopic ellipsometry methods. For the initial purpose of adding new
41
42
43 inputs to the ellipsometry model, focused ion-beam tomography experiments were
44
45
46 conducted to extract porosity/depth profiles of these systems. To reproduce the optical
47
48
49 free-carrier behaviour in the infrared, the ellipsometric data acquired were fitted to an
50
51
52
53
54
55 anisotropic Bruggeman model including Tauc-Lorentz and Drude oscillators, which
56
57
58
59
60

1
2
3 enabled the determination of carrier density and in-grain mobility. The nice agreement of
4
5
6
7 these results with those obtained by combining Hall effect measurements, X-ray
8
9
10 diffraction and transmission electron microscopy studies supported the validity of the
11
12
13 proposed method, opening new horizons in the characterization of nanowire-based
14
15
16
17 semiconducting layers.
18
19
20
21
22
23
24
25
26
27
28
29
30
31
32
33
34
35
36
37
38
39
40
41
42
43
44
45
46
47
48
49
50
51
52
53
54
55
56
57
58
59
60

INTRODUCTION

Gallium nitride (GaN) nanowire (NW) arrays grown by plasma-assisted molecular beam epitaxy (PAMBE) have recently attracted the attention of the scientific community due to their high crystalline quality and low defect density¹⁻⁴ and their unique electrical and optical properties⁵⁻⁷. By tuning the growth conditions, the size and arrangement of the nanowires, and thus the porosity, can be controlled so as to modulate the optical and electrical properties of the system^{5,8-11}. Thanks to its high surface-to-volume ratio, tuneable refractive index and bandgap, high light extraction efficiency and quantum efficiency, GaN arrays have been erected as a promising material not only for the development of optoelectronic and optical devices such as field-effect transistors (FETs)^{12,13}, light-emitting diodes (LEDs)^{6,14}, laser diodes¹⁵ and detectors¹⁶, but also for photo-electrochemical water splitting^{17,18} and energy storage¹⁹ applications.

While the optical characterization of GaN nanowire and nanorod arrays through spectroscopic ellipsometry (SE)^{9,10}, polarized-goniometry²⁰ or reflectivity spectroscopy¹¹ is well reported in the literature, the characterization of electrical properties related to conductivity, like carrier concentration and mobility, presents some difficulties associated to the geometry of this kind of structures^{4,21}. Up to now, the majority of the studies are focused on Hall effect and field effect measurements performed on single nanowires after fabricating multiple contacts²²⁻²⁵. However, given the challenges aforementioned, very few studies based on the electrical characterization of complete nanowire films have been reported at the time of the submission of this work²⁶⁻²⁸. Hence, the development of novel and alternative methodologies for the electrical characterization of nanowire layers, such as noncontact THz spectroscopic measurements²⁹, is crucial.

1
2
3 In this work, we report an alternative and straightforward way for both optical and electrical
4 characterization of high-quality single crystalline GaN self-assembled NW films by means of
5 visible-IR spectroscopic ellipsometry (SE), which is a cheap, fast, and non-destructive technique
6 that can be used as a systematic characterization tool even for industrial processes. These porosity-
7 controlled layers of GaN nanostructures were grown in a compact fashion by PAMBE. The
8 porosity profiles along the layer thickness, which are not constant due to the presence of different
9 nanostructures shapes from solid (SNW) to c-shape (CNW) and hollow (HNW) nanowires, were
10 extracted through focused ion-beam (FIB) tomography reconstructions (slice and view). In order
11 to reproduce the SE measurements, these porosity profiles were incorporated into an optical model
12 through an effective-medium approximation in the framework of an anisotropic Bruggeman
13 model, in which the optical constants of GaN are modelled by a combination of a Tauc-Lorentz
14 oscillator and a Drude oscillator. This approach not only allows to determine porosity, thickness
15 and optical constants of GaN NW films but also carrier densities and optical mobilities. The
16 validity of the defined model is supported by combining Hall effect measurements, X-ray
17 diffraction (XRD) and transmission electron microscopy (TEM) techniques including high-
18 resolution (HRTEM) and energy-dispersive X-ray spectroscopy (EDX).
19
20
21
22
23
24
25
26
27
28
29
30
31
32
33
34
35
36
37
38
39
40

41 **EXPERIMENTAL SECTION**

42
43
44 Wurtzite GaN nanowire layers were grown on chemically cleaned p-type Si(111) or (100)
45 substrates by PAMBE along the [0001] direction, and epitaxially aligned with the underlying Si
46 substrate, following the same procedure as the one described in a previous study¹⁰. For 3D
47 reconstructions, two different systems were used to acquire FIB-SEM tomography datasets: a
48 Scios 2 DualBeam microscope from Thermo Scientific and a CrossBeam 350 microscope from
49 ZEISS. Those datasets consist of stacks of SEM images recorded using backscattered electrons
50
51
52
53
54
55
56
57
58
59
60

1
2
3 and an acceleration voltage of 1.4 kV. The optical and electrical properties of each sample were
4
5 evaluated by standard vis-IR spectroscopic ellipsometry at incident angles of 65°, 75° and 85°.
6
7 These measurements were performed with a J. A. Woollam M2000XI (from 400 to 1700 nm) J.
8
9 A. Woollam IR-VASE Mark II (from 1700 to 24000 nm), respectively. In order to confirm the
10
11 veracity of the electrical properties obtained through vis-IR SE experiments, room temperature
12
13 Hall Effect measurements were conducted using a Van der Pauw Ecopia AMP-55 Hall
14
15 measurement system in the presence of a magnetic field. The crystallographic structure was
16
17 investigated by X-ray diffraction (XRD) experiments which were performed using a Seifert XRD
18
19 3000 diffractometer fitted with a copper source and a 1 mm beam collimator. To obtain additional
20
21 insights into the nanostructure, high-resolution transmission electron microscopy (TEM)
22
23 experiments were conducted in a FEI Talos F200S analytical microscope operated at 200 kV and
24
25 equipped with a Super-X energy-dispersive X-ray spectrometry (EDX) system that includes two
26
27 silicon drift detectors. Local compositional analyses were performed by combining high-angle
28
29 annular dark-field imaging (HAADF) and EDX acquisitions using the scanning (STEM) mode.
30
31 Electron-transparent cross-sectional FIB lamellae were prepared for TEM observations by using
32
33 the aforementioned FIB systems.
34
35
36
37
38
39
40

41 **RESULTS AND DISCUSSION**

42
43
44 With the additional purpose of examining the effect of substrate orientation on optical and
45
46 electrical properties, the samples selected for this study were T2 and T2' (following the
47
48 nomenclature of Ref. 10), i.e., the same growth conditions but different substrate orientations:
49
50 Si(111) and Si(100), respectively.
51
52
53
54
55
56
57
58
59
60

1
2
3 These two samples are composed by a mixture of three different kind of NWs: SNWs filled and
4 with hexagonal facets, HNWs, with solid bases which evolve into hollow structures when reaching
5 a critical thickness, and CNWs, similar to HNWs but partially opened longitudinally. More in-
6 depth studies of the structure and morphology of these three types of nanowires as well as the
7 effect that growth conditions have on both the overall porosity and the optical properties of such
8 systems can be found in Ref. 10. Due to the presence of this variety of nanostructures, the porosity
9 profile along the Z direction turns uncertain and non-linear, hindering the optical characterization
10 of these systems³⁰. In order to overcome this difficulty, representative areas of T2 and T2' samples
11 were explored with the aim of extracting their porosity profiles by performing FIB tomography
12 experiments. In this regard, two different FIB systems (Thermo Scientific Scios 2 DualBeam and
13 ZEISS CrossBeam 350) were employed to carry out 3D reconstructions and analyses of T2 and
14 T2' volumes, respectively (see Supporting Information Section I for a detailed description of the
15 experimental data acquisition, segmentation, 3D reconstruction and porosity profile extraction).
16
17
18
19
20
21
22
23
24
25
26
27
28
29
30
31
32
33
34
35
36
37
38
39
40
41
42
43
44
45
46
47
48
49
50
51
52
53
54
55
56
57
58
59
60

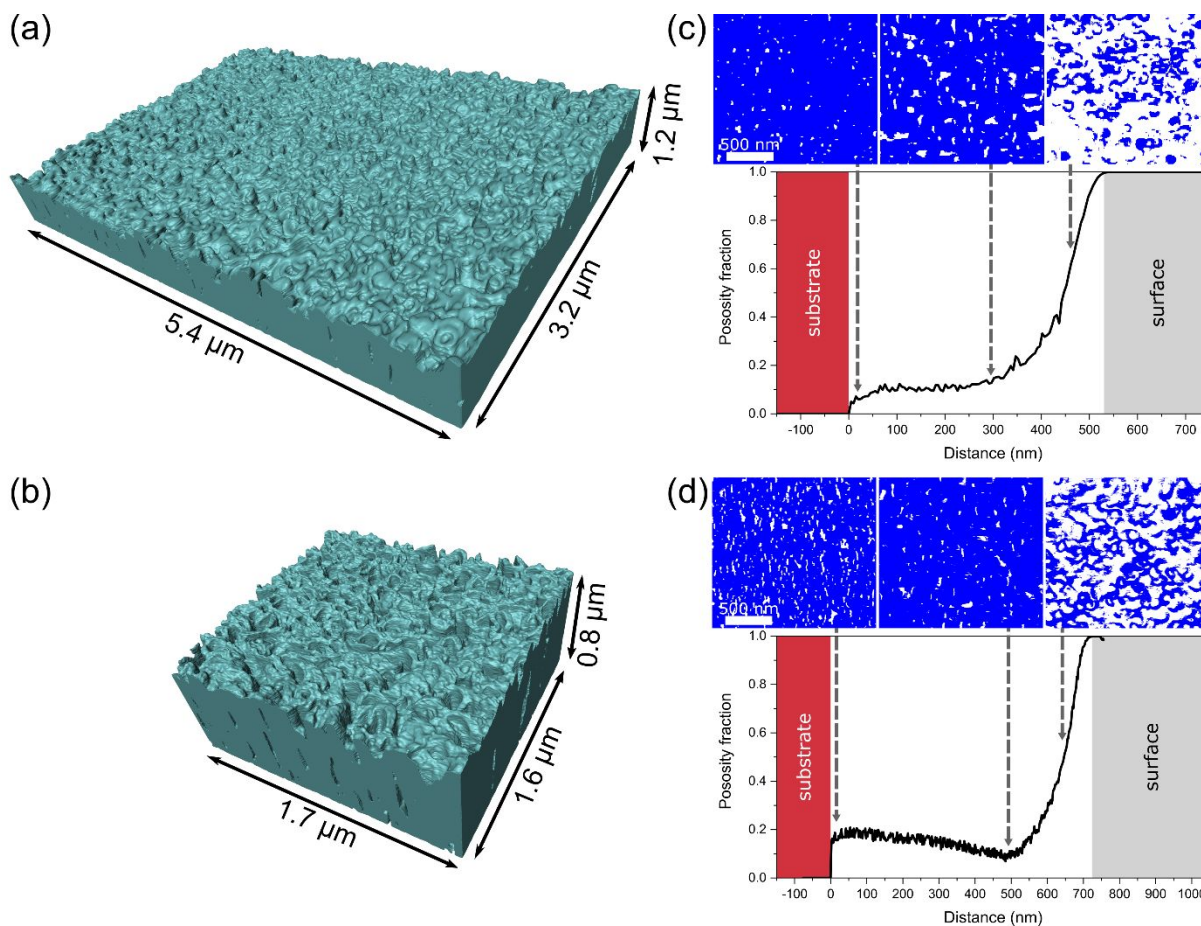


Figure 1. 3D reconstructions of the NW arrays in (a) T2 and (b) T2' samples through FIB tomography. Volume sizes are $5440 \times 3222 \times 1230 \text{ nm}^3$ and $1744 \times 1602 \times 834 \text{ nm}^3$, respectively. Porosity profiles of (c) T2 and (d) T2' samples extracted along the surface normal together with some planar views obtained by data segmentation at different depths (GaN material and voids are shown in blue and white colors, respectively). Note that these images were cut to show the same field of view in both samples, for comparison.

1
2
3
4
5
6
7
8
9
10
11
12
13
14
15
16
17
18
19
20
21
22
23
24
25
26
27
28
29
30
31
32
33
34
35
36
37
38
39
40
41
42
43
44
45
46
47
48
49
50
51
52
53
54
55
56
57
58
59
60

Figures 1(a) and (b) display volume visualizations of T2 and T2' samples respectively together with their porosity profiles along the surface normal (Fig. 1(c-d)). Note that the planar views obtained by data segmentation at depths close to the surface reveal the characteristic morphologies of GaN NWs (SNW, HNW and CNW). As a first approach, it can be appreciated a significant difference between the porosity profiles of both specimens. Whereas one of them (T2) experiences a first stage in which the porosity remains constant with the depth, followed by a progressive increase in porosity; the other (T2') firstly experiments a slight decrease in porosity up to reaching a critical thickness from which it increases sharply. Furthermore, there are also differences in the total thickness of both samples (around 550 nm and 750 nm for T2 and T2', respectively). In this way, the shapes of these two profiles only can be explained by considering that nanowires are composed by solid (filled) bases that evolve (or not) into hollow structures (HNW or CNW), justifying the initial step of constant porosity (first 300 nm of thickness) in sample T2. These results are consistent with the assumptions made in previous works¹⁰. On the other hand, the preliminary drop in porosity in sample T2' could be associated with the broadening of solid bases that occurs after attaining 100-150 nm thickness.

Once known the evolution of the porosity along the NW layer, vis-IR SE experiments were performed in areas close to 3D reconstructions with the purpose of conducting a full, accurate and comparable characterization of these systems. To do so, visible and infrared spectroscopic ellipsometry measurements were performed at incidence angles of 65°, 75° and 85°. Both spectra were acquired separately and then were spliced and treated with the WVASE software from J.A. Woollam. In a first stage of the study, the data acquired were fitted to an Anisotropic Bruggeman Effective Medium Approximation (ABEMA) model composed by a mixture of wurtzite GaN,

1
2
3 whose optical constants are modelled by the ones obtained for high-quality single-crystalline α -
4 GaN layers³¹, and void. A 2-nm-thick layer of silicon nitride (Si_3N_4) located between the Si
5
6 substrate and the nanowire layer was also included in the optical model. With the aim of reflecting
7
8 the columnar geometry of the film with NWs growing perpendicular to the substrate, the
9
10 depolarization factor in the extraordinary (out-of-plane) direction (q_z) was fixed to 0, whereas the
11
12 ordinary or in-plane ones (q_x and q_y) were fixed at 1/2 (uniaxial anisotropy)^{32,33}. Moreover, the
13
14 porosity profiles extracted by FIB tomography 3D reconstructions were incorporated into the
15
16 model in order to reproduce the variation in the refractive index (n) along the Z direction (as a
17
18 function based graded-index layer). On the other side, the anisotropy associated to the wurtzite
19
20 GaN structure was considered negligible compared to the anisotropy associated to the columnar
21
22 structure. Indeed, wurtzite GaN has a uniaxial structure, and its intrinsic birefringence, which is
23
24 the difference $\Delta n = n_z - n_{x,y}$ between extraordinary optical index n_z and ordinary one $n_{x,y}$ is of the
25
26 order of 0.02 (in absolute terms) in the visible range according to Ref. 31 (see Supporting
27
28 Information Figure S8). On the other hand, by modelling GaN as an isotropic material and
29
30 implementing it into the ABEMA model above mentioned, the birefringence in the visible range
31
32 is around 0.1 in the visible range as one can see on Figure 2(c) and 2(d), that is, 5 times higher
33
34 than the intrinsic birefringence of wurtzite GaN. We may therefore neglect the intrinsic uniaxial
35
36 structure of GaN, and conclude that the observed anisotropy is mainly due to the elongated shape
37
38 of the NWs.
39
40
41
42
43
44
45
46
47

48 Despite this model provides a fine agreement to the experimental data in the visible range, it fails
49
50 to reproduce the absorption in the IR range, as can be seen on Figure 2(a) and 2(b). Indeed, the
51
52 presence of a weak but non-negligible level of doping in the GaN results in free carrier absorption
53
54 in the IR range. In order to model correctly this absorption, we replace the tabulated optical
55
56
57
58
59
60

1
2
3 constants from Ref. 31 for wurtzite GaN by a combination of two oscillators: (i) a Tauc-Lorentz
4 Oscillator (TLO) modelling the direct band gap (E_g) absorption of GaN³⁴; and (ii) a Drude
5 Oscillator (DO) modelling the free-carrier behaviour in the IR range³⁵ (a scheme of the optical
6 model is presented in Supporting Information Figure S2). From 1.5 to 3 eV, that is, in the visible
7 range, the parameters of the TLO were adjusted onto the values of the dielectric constants for
8 wurtzite GaN from the Ref. 31. The advantage of using a Tauc-Lorentz oscillator over, e.g., a
9 simple Lorentz oscillator is to impose a more realistic value of zero for ϵ_2 below the gap. Also, a
10 TLO permits the combination with another oscillator, here a Drude oscillator, unlike, e.g., a simple
11 Cauchy model. In this way, a DO was incorporated to represent free-carrier absorption by fitting
12 the ellipsometry data in the lower energy region, considering an effective mass (m^*) of 0.20 for
13 wurtzite GaN³⁶, while the free carrier density $N_{e(opt)}$ and optical mobility μ_{opt} are the parameters
14 to be fitted. Indeed, the Drude model is appropriate to characterize samples with carrier
15 concentrations down to 10^{18} cm⁻³ when infrared spectroscopic ellipsometry is used³⁷.

16
17
18
19
20
21
22
23
24
25
26
27
28
29
30
31
32
33
34 The fittings obtained for T2 and T2' samples after incorporating TLO and DO models are shown
35 in Fig. 2(a) and (b) respectively, together with the fitting obtained by using either a TLO alone
36 (TLO) or the data from Ref. 31 (Adachi) for GaN. As one can see, a TLO alone or Adachi data
37 provide a quite good description of the measured Ψ and Δ SE values in the visible range. However,
38 while approaching the IR range, a shift in energy between the modelled and measured oscillations
39 of Ψ and Δ is noticeable. Moreover, they predict oscillations below 0.4 eV that are not observed.
40
41
42
43
44
45
46
47
48
49
50
51
52
53
54
55
56
57
58
59
60
The addition of a Drude oscillator to the model resolves these issues: the modelled oscillations of
 Ψ and Δ remain in phase with the measured ones even in the IR range, and their cut-off at 0.4 eV
is correctly predicted. We emphasize here that this cut-off provides a very robust criterion to fit
the carrier density: the Mean Square Error (MSE) increases by 10% when a relative change of 10%

of $N_{e(opt)}$ is applied to the model (see Supporting Information Figure S6). With this criterion, the relative uncertainty on the fitted value of $N_{e(opt)}$ is $\pm 10\%$, for values of $N_{e(opt)}$ as low as 1×10^{18} e/cm^3 . That is, $\pm 0.1 \times 10^{20}$ e/cm^3 for a fitted value of $N_{e(opt)} = 1.3 \times 10^{20}$ e/cm^3 for sample T2.

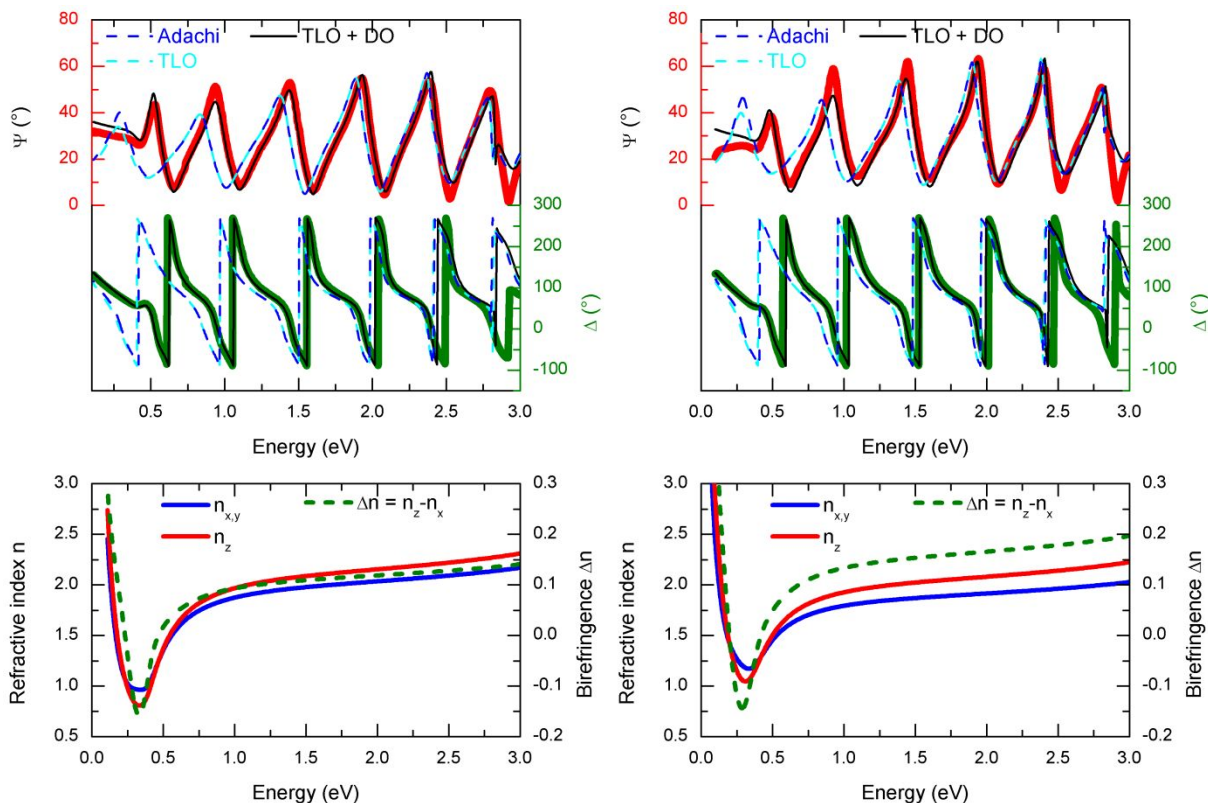


Figure 2. Measured spectroscopic ellipsometry angles Ψ (red) and Δ (green) for (a) T2 and (b) T2' samples at an incident angle of 65° . Thick solid lines represent the experimental measurements. Thin solid black lines represent the best-fit achieved using the SE model (ABEMA including TLO + DO). For comparison, dashed lines represent the best-fit obtained with an ABEMA model with only a TLO (light blue) or using Adachi et al. (Ref. 31) data (dark blue) for GaN. In-plane (blue solid lines) and out-of-plane (red solid lines) refractive indices and

1
2
3 birefringence (dashed green lines) of (c) T2 and (d) T2' samples obtained from simulations using
4
5 the SE model.
6
7
8
9

10
11 The evolutions of the in-plane and out-of-plane refractive indices along with the birefringence of
12 T2 and T2' NW layers, obtained from the enhanced ellipsometry model over the vis-IR range, are
13 displayed in Fig. 2(c) and (d), respectively. As expected, the refractive indices of both samples in
14 the visible spectrum are smaller than that of bulk GaN due to the presence of voids. Nevertheless,
15 both layers start to experience a metallic behaviour at energies around 0.4 eV which corresponds
16 to the onsets of free-carrier absorption, leading to an increase in refractive indices. Also note that,
17 from visible to near infrared, the refractive indices in the *Z* direction are greater than that
18 corresponding to the in-plane one. Likewise, the values of birefringence obtained in this spectral
19 range let us evidence that the optical anisotropy in T2' is stronger than in T2.
20
21
22
23
24
25
26
27
28
29
30
31
32

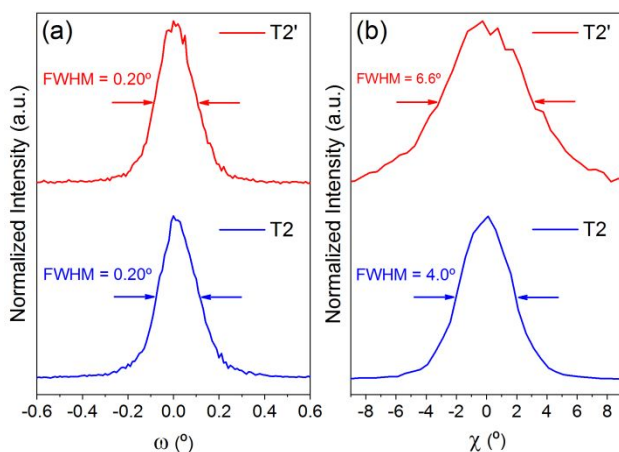
33 Additionally, the DO parameters ($N_{e(opt)}$ and μ_{opt}) provided by the SE model are $N_{e(opt)}(T2) = (1.3$
34 $\pm 0.1) \times 10^{20} \text{ e}^-/\text{cm}^3$ and $\mu_{opt}(T2) = 45 \pm 5 \text{ cm}^2/\text{V}\cdot\text{s}$; $N_{e(opt)}(T2') = (1.1 \pm 0.1) \times 10^{20} \text{ e}^-/\text{cm}^3$ and μ_{opt}
35 $(T2') = 34 \pm 5 \text{ cm}^2/\text{V}\cdot\text{s}$. Note that the doping level of both samples is surprisingly high, taking into
36 account that they were not intentionally doped. Regarding the optical mobility, the values extracted
37 from the SE model are in good agreement with the electrical mobility obtained in the literature by
38 four-point measurement for single GaN NWs^{4,38}. Besides, these results are also consistent with the
39 values of mobility obtained from the Hilsum equation³⁹ adapted for the case of GaN NWs⁴⁰, that
40 is, 32.2 cm²/V·s for T2 and 33.2 cm²/V·s for T2' considering the doping level predicted by the SE
41 model. This is because the optical measurements performed supply intra-granular information,
42 which is equivalent to the mean of a set of measurements carried out on different single NWs.
43
44
45
46
47
48
49
50
51
52
53
54
55
56
57
58
59
60

In order to confirm the values of carrier density and mobility predicted by SE as well as to validate the defined model, room temperature Hall Effect measurements were conducted. For this purpose, four contacts were placed at the corners of squared-shaped samples which were cut in such way that the same areas as in previous experiments were studied.

	Sample T2	Sample T2'
Hall voltage, V_H (V)	$(-4.4 \pm 0.2) \cdot 10^{-6}$	$(-4.4 \pm 0.9) \cdot 10^{-6}$
Sheet Resistance, R_s (Ω)	111.5 ± 0.1	1881.2 ± 6.0
Hall carrier density, $N_{e(Hall)}$ (e^-/cm^3)	$(1.6 \pm 0.1) \cdot 10^{20}$	$(1.2 \pm 0.3) \cdot 10^{20}$
Hall mobility, μ_{Hall} ($\text{cm}^2/\text{V}\cdot\text{s}$)	6.8 ± 0.3	0.4 ± 0.1
Optical carrier density, $N_{e(opt)}$ (e^-/cm^3)	$(1.3 \pm 0.1) \cdot 10^{20}$	$(1.1 \pm 0.1) \cdot 10^{20}$
Optical mobility, μ_{opt} ($\text{cm}^2/\text{V}\cdot\text{s}$)	45 ± 5	34 ± 5

Table 1. Summary of the electrical characterization of T2 and T2' samples through Hall Effect measurements and vis-IR SE. Hall effect experiments were conducted by supplying a current of 100 μA and inducing a magnetic field of 0.58 T. The thicknesses considered for these calculations were the obtained from 3D reconstructions (Fig. 1).

An overview of the results obtained from the Hall effect measurements for T2 and T2' samples can be found in Table.1. The negative sign of the Hall voltage indicates that the majority of the carriers were electrons for both samples (n-type semiconductor). Moreover, the values of carrier densities measured are in accordance with those predicted by SE, which confirms the high n-doping level. However, great differences between the electrical behaviour of T2 and T2' samples are observed. As can be seen, sample T2' exhibits a greater opposition to the flow of electric current than T2 (just over one order of magnitude). It should be also noted that the mobility measured by Hall effect, in addition to be surprisingly low, does not correspond with the one predicted by the SE model. The latter is expectable since SE provides information related to the free-carrier mobility within grains (μ_{opt}) while Hall effect give us information about the total mobility of the layer (μ_{Hall}), including the effects of grain boundaries as well as the porosity of the structure. Conversely, $N_{e(Hall)}$ values are not affected by the porosity⁴¹, so it is relevant to compare them directly with those resulting from SE ($N_{e(opt)}$). Thus, μ_{Hall} values suggest that the mobility in GaN NW arrays is dominated by inter-grain barriers.



1
2
3
4 **Figure 3.** XRD rocking curves: (a) ω -scans and (b) χ -scans of the GaN 0002 reflection for
5
6
7 T2 (blue lines) and T2' (red lines) samples.
8
9

10
11
12
13
14 This assumption is also supported by the shape analyses of XRD rocking curves (ω and χ -scans)
15
16 of 0002 GaN diffraction peaks. As can be appreciated in Fig. 3(a), the full width at half maximum
17
18 (FWHM) values of the ω -scans are rather small for T2 and T2' samples (0.20° in both cases) which
19
20 not only indicates the good crystal quality of nanowires (low density of dislocations) but also a
21
22 good epitaxial alignment between the GaN nanostructure and the single-crystalline Si substrate
23
24 (the out-of-plane epitaxial relationship is GaN(0001)||Si(111) for T2 and GaN(0001)||Si(001) for
25
26 T2'). In addition, χ -scans (Fig. 3(b)) reveal that the slight misorientation of the (0002) planes along
27
28 the growth direction (tilt) is more significant in T2' than in T2.
29
30
31
32

33
34 Once come to this point, it is time to account for the unintentional high doping concentration of
35
36 the GaN NW layers. With the aim of elucidating the origin of the doping, EDX chemical analyses
37
38 were carried out in both samples. The Thermo Scientific Velox™ user interface was used for data
39
40 acquisition and processing. Quantification of the EDX data was performed using the standardless
41
42 method. In order to minimize errors during this step, intensities of the different peaks were
43
44 extracted with a great care after background subtraction with a multi-polynomial approach. Since
45
46 this approach can lead to inaccuracy in the quantitative composition determination, especially for
47
48 low Z elements like O and N, qualitative analyses were conducted. STEM high-angle annular dark
49
50 field imaging (HAADF) and EDX elemental maps (see Fig. 4(a-b)) reveal a remarkable presence
51
52 of oxygen distributed throughout both films. Note that the oxygen signal becomes greater on the
53
54
55
56
57
58
59
60

edges of the nanowires, where projections only bring contributions of the surrounding material, suggesting that oxygen is mainly accumulated at NW surfaces (see elemental profiles obtained for both samples in Figure 5(a-b)). Likewise, EDX normalized spectra (Fig. 4(c)) of both samples reveal that the amount of oxygen in T2' is larger than the one detected in T2. In this context, it is well known that high concentrations of oxygen in GaN can cause high levels of electron concentration^{42–45}. Therefore, in consideration of these results, it could be assumed that the observed GaN NWs doping is linked to oxygen impurities.

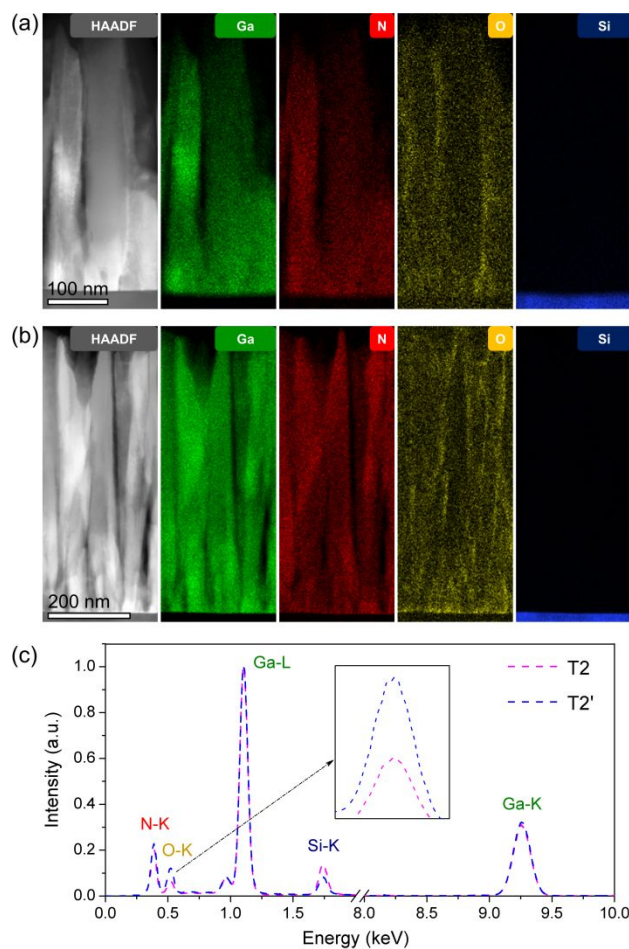


Figure 4. STEM-HAADF and EDX elemental maps of (a) T2 and (b) T2' samples obtained for Ga, N, O and Si atoms. (c) EDX spectra, normalized at Ga-L_α peak (1098 eV), for T2

1
2
3 (magenta dashed line) and T2' (blue dashed line) samples. The inset corresponds to the
4
5
6
7 feature of the O-K_α peak (525 eV).
8
9
10
11
12
13

14 By contrast, the explanation for the low total mobility of such GaN nanostructures is more
15
16 complex. In addition to the effect of porosity, which acts by reducing the volume in which the
17
18 current flows⁴⁶, two additional reasons could contribute to this phenomenon: (i) surface state
19
20 trapping; and (ii) the formation of native oxide on the surface. Generally, electrical properties of
21
22 nanowire-structured semiconductors are sensitive to the status of their surfaces. One of the main
23
24 problems of nanostructured systems is the decrease in the carrier mobility due to the scattering
25
26 from the surface states. Furthermore, this effect becomes even more significant for the case of
27
28 NWs because of their high surface-to-volume ratio, which leads to free carriers within the wire
29
30 being trapped at surface traps^{16,47}. Nonetheless, this phenomenon would only affect the mobility
31
32 inside nanowires which was proved not to be the responsible for the low total mobility of the
33
34 studied systems.
35
36
37
38
39
40
41
42
43
44
45
46
47
48
49
50
51
52
53
54
55
56
57
58
59
60

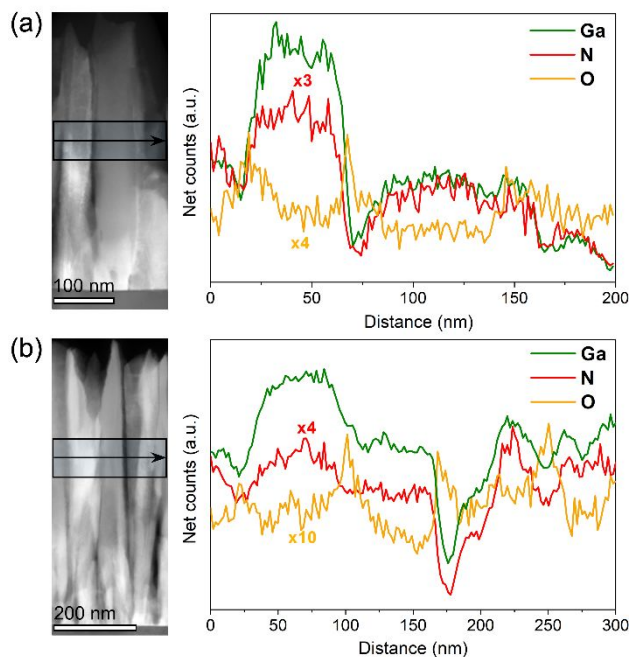


Figure 5. STEM-HAADF and Ga, N and O EDX elemental profiles for (a) T2 and (b) T2' samples.

Note that such profiles were integrated across the NWs following the direction indicated by the arrows.

Another consequence of the great surface-to-volume ratio is the formation of amorphous layers of native oxide surrounding the nanowires when they are exposed to air. This issue has been previously reported by other authors^{21,48} resulting in a detrimental effect on electrical properties since this oxide shell acts as a barrier for the motion of electrons among nanowires. According to similar studies^{49,50}, this fact might also provide an explanation for the high levels of electron concentration in these GaN nanostructures: part of the oxygen atoms could diffuse from the oxide layer into the GaN nanowire at room temperature, originating oxygen impurities. HRTEM micrographs and fast Fourier transform (FFT) diffractions of isolated wurtzite GaN nanowires of T2 (Fig. 6(a)) and T2' (Fig. 6(b)) samples evidence this formation of amorphous layers of native

1
2
3 oxide on the surface. Note that the amount of oxide generated on the surface of the nanowire
4
5 belonging to T2' is considerably larger than that observed in the NW of T2. The latter, in addition
6
7 to supporting the results obtained through EDX analyses, could be associated to a major
8
9 susceptibility to oxidation of T2' compared to T2 sample, leading to a minor mobility of the T2'
10
11 sample as Hall effect measurements revealed. Thus, we propose that both the native oxide layer
12
13 formed on cylinder-like surfaces and porosity are the limiting factors on the global mobility of
14
15 GaN nanowire arrays films.
16
17
18
19
20
21
22
23
24
25
26
27
28
29
30
31
32
33
34
35
36
37
38
39
40
41
42
43
44
45
46
47
48
49
50
51
52
53
54
55
56
57
58
59
60

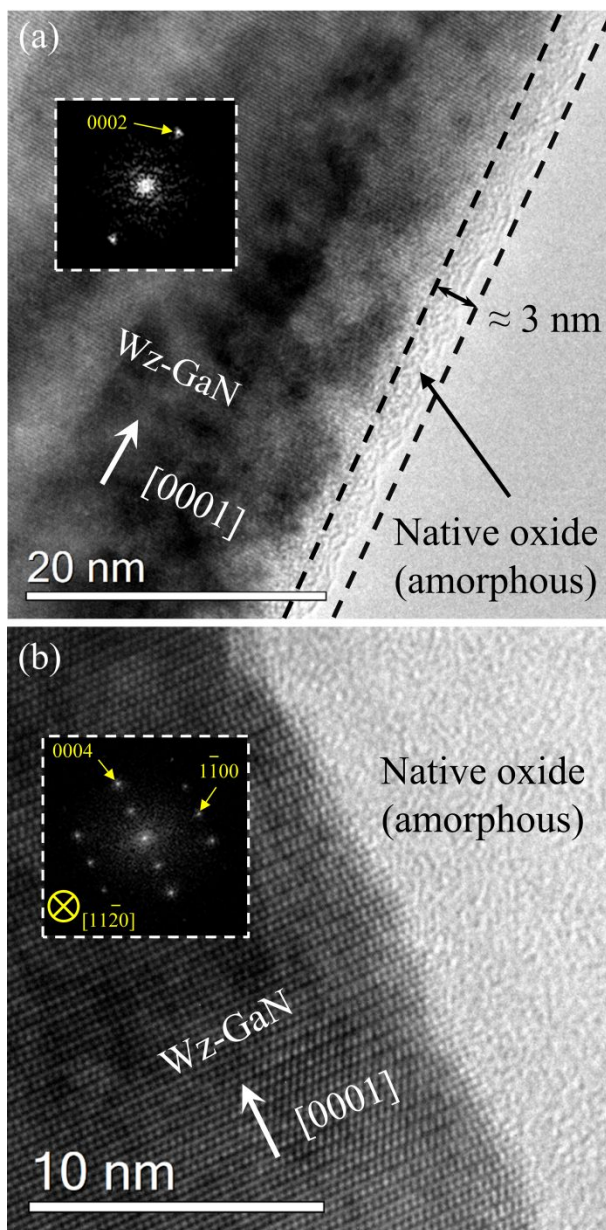


Figure 6. High-resolution TEM micrographs and corresponding FFT diffractions of single nanowires of (a) T2 and (b) T2' samples. Note that these TEM observations were conducted on two FIB lamellae prepared by using the same SEM-FIB systems as for FIB tomography experiments.

1
2
3
4
5
6 After reaching these conclusions, it is clear that surface-to-volume ratio plays a vital role in both
7
8 optical and electrical properties of GaN NW arrays. The insertion of porosity allows to cut down
9
10 the effective refractive index of the layer. However, increasing the porosity implies greater surface-
11
12 to-volume ratios, which has been proved to have a detrimental effect on the electron mobility
13
14 because the formation of native oxide shells within the semiconducting layers is favoured when
15
16 the surface exposed to air is greater⁵¹. Hence, by tuning the growth conditions, the porosity of the
17
18 nanostructures can be controlled, making these systems more appropriate for optical or electrical
19
20 applications.
21
22
23
24

25 **CONCLUSIONS**

26
27
28 In summary, optical and electrical properties of GaN nanowire arrays grown on Si (111) and Si
29
30 (100) by PAMBE were simultaneously explored by means of an innovative methodology based
31
32 on vis-IR spectroscopic ellipsometry. For a better description of these nanostructures, porosity
33
34 profiles extracted by FIB tomography reconstructions were implemented into an ABEMA model
35
36 where the optical constants of GaN were modelled by a multioscillator approach (TLO and DO)
37
38 which enabled us to determine the carrier density and intra-grain mobility of such nanostructures.
39
40 These results evidenced electron concentrations of about 10^{20} cm⁻³ and optical mobilities
41
42 comparable to the one reported for individual GaN nanowires (30-50 cm²/V·s). Hall effect
43
44 measurements, XRD and transmission electron microscopy (STEM-EDX and HRTEM) studies
45
46 not only provided a confirmation of the results predicted by the SE model but also let us elucidate
47
48 that the oxygen impurity was the responsible for the high doping level and that the total mobility
49
50
51
52
53
54
55
56
57
58
59
60

1
2
3 of such GaN arrays was mainly limited by the combined effect of porosity and surface oxidation
4
5 of individual nanowires.
6
7
8
9
10

11 ASSOCIATED CONTENT

16 Supporting Information.

17
18
19
20 Three-dimensional FIB-SEM tomography reconstructions (experimental data
21
22
23
24 acquisition; data processing; alignment, rotation, cropping and denoising; segmentation
25
26
27 and porosity quantification), optical modeling (optical model; fitting procedure; relevance
28
29
30 of the Drude Oscillator; lowest detectable carrier concentration; uncertainty of the fit
31
32
33
34 parameters; intrinsic anisotropy of GaN; plasmonic effects) and additional references.
35
36
37
38
39
40

41 AUTHOR INFORMATION

45 Corresponding Author

46
47
48
49 * Email: fmiguel.morales@uca.es
50
51
52
53

54 Present Addresses

1
2
3 † Present address: Solid State Physics, Lund University, Box 118, S-221 00 Lund,
4
5
6
7 Sweden.

11 Author Contributions

12
13
14
15 The manuscript was written through contributions of all authors. All authors have given
16
17
18 approval to the final version of the manuscript.
19
20
21
22
23
24
25
26

27 ACKNOWLEDGMENTS

28
29
30
31 The authors would like to express their gratitude to Ellen Backen, applications scientist
32
33
34 from Thermo Fisher Scientific, for the images registered at the Scios 2 HiVac system at
35
36
37 Nanoport (Eindhoven). We would also like to acknowledge ZEISS corporations for
38
39
40 technical assistance as well as the loaning of the CrossBeam 350 system and the data
41
42
43 acquisition. A. J. Santos would like to thank the IMEYMAT Institute and the Spanish
44
45
46 Ministerio de Educación y Cultura for the concessions of grants (ICARO-173873 and
47
48
49 FPU16-04386). The “Talent Attraction Program” of the University of Cádiz is
50
51
52 acknowledged by supporting B. Lacroix contract code E-11-2017-0117214. University of
53
54
55
56
57
58
59
60

1
2
3 Cádiz and IMEYMAT are also agreed by financing the mutual facilities available at the
4
5
6
7 UCA R&D Central Services (SC-ICYT), the UCA project reference “PUENTE PR2018-
8
9
10 040”, and the IMEYMAT project reference “AGREGADOR 2018-1”. The authors would
11
12
13
14 like to acknowledge the financial support provided by Sêr Cymru National Research
15
16
17
18 Network in Advanced Engineering and Materials. This work was also supported by the
19
20
21 IMATOP project funded by “Nouvelle Aquitaine” Region and by the European Structural
22
23
24 and Investment Funds (ERDF reference P-2016-BAFE-209).
25
26
27
28
29
30

31 REFERENCES

- 32
33
34
35 (1) Sobanska, M. Comprehensive Analysis of the Self-Assembled Formation of GaN
36
37
38 Nanowires on Amorphous Al_xO_y : In Situ Quadrupole Mass Spectrometry Studies.
39
40
41
42 *Nanotechnology* **2019**, *30* (15), 154002.
43
44
45
46 (2) Bolshakov, A. D.; Mozharov, A. M.; Sapunov, G. A.; Shtrom, I. V.; Sibirev, N. V.;
47
48
49
50 Fedorov, V. V.; Ubyivovk, E. V.; Tchernycheva, M.; Cirlin, G. E.; Mukhin, I. S.
51
52
53
54 Dopant-Stimulated Growth of GaN Nanotube-like Nanostructures on Si(111) by
55
56
57
58
59
60

- 1
2
3 Molecular Beam Epitaxy. *Beilstein J. Nanotechnol.* **2018**, *9* (1), 146–154.
4
5
6
7
8 (3) Schlager, J. B.; Sanford, N. A.; Bertness, K. A.; Barker, J. M.; Roshko, A.;
9
10
11 Blanchard, P. T. Polarization-Resolved Photoluminescence Study of Individual
12
13
14 GaN Nanowires Grown by Catalyst-Free Molecular Beam Epitaxy. *Appl. Phys. Lett.*
15
16
17
18 **2006**, *88* (21), 1–4.
19
20
21
22
23 (4) Mansfield, L. M.; Bertness, K. A.; Blanchard, P. T.; Harvey, T. E.; Sanders, A. W.;
24
25
26 Sanford, N. A. GaN Nanowire Carrier Concentration Calculated from Light and Dark
27
28
29 Resistance Measurements. *J. Electron. Mater.* **2009**, *38* (4), 495–504.
30
31
32
33
34 (5) Pauzauskie, P. J.; Yang, P. Nanowire Photonics. *Mater. Today* **2006**, *9* (10), 36–
35
36
37
38 45.
39
40
41
42 (6) Chen, C. Y.; Zhu, G.; Hu, Y.; Yu, J. W.; Song, J.; Cheng, K. Y.; Peng, L. H.; Chou,
43
44
45
46 L. J.; Wang, Z. L. Gallium Nitride Nanowire Based Nanogenerators and Light-
47
48
49 Emitting Diodes. *ACS Nano* **2012**, *6* (6), 5687–5692.
50
51
52
53
54 (7) Barrigón, E.; Heurlin, M.; Bi, Z.; Monemar, B.; Samuelson, L. Synthesis and
55
56
57
58
59
60

- 1
2
3 Applications of III–V Nanowires. *Chem. Rev.* **2019**, *119*(15), 9170–9220.
4
5
6
7
- 8 (8) Park, Y. S.; Lee, G.; Holmes, M. J.; Chan, C. C. S.; Reid, B. P. L.; Alexander-
9
10
11 Webber, J. A.; Nicholas, R. J.; Taylor, R. A.; Kim, K. S.; Han, S. W.; et al. Surface-
12
13
14
15 Effect-Induced Optical Bandgap Shrinkage in GaN Nanotubes. *Nano Lett.* **2015**, *15*
16
17
18 (7), 4472–4476.
19
20
21
22
- 23 (9) Lee, J. H.; Lee, B.; Kang, J. H.; Lee, J. K.; Ryu, S. W. Optical Characterization of
24
25
26 Nanoporous GaN by Spectroscopic Ellipsometry. *Thin Solid Films* **2012**, *525*, 84–
27
28
29
30 87.
31
32
33
- 34 (10) Gómez, V. J.; Santos, A. J.; Blanco, E.; Lacroix, B.; García, R.; Huffaker, D. L.;
35
36
37
38 Morales, F. M. Porosity Control for Plasma-Assisted Molecular Beam Epitaxy of
39
40
41
42 GaN Nanowires. *Cryst. Growth Des.* **2019**, *19*(4), 2461–2469.
43
44
45
- 46 (11) Chen, H.-Y.; Lin, H.-W.; Wu, C.-Y.; Chen, W.-C.; Chen, J.-S.; Gwo, S. Gallium
47
48
49 Nitride Nanorod Arrays as Low-Refractive-Index Transparent Media in the Entire
50
51
52
53 Visible Spectral Region. *Opt. Express* **2008**, *16*(11), 8106.
54
55
56
57
58
59
60

- 1
2
3
4 (12) Cha, H. Y.; Wu, H.; Chandrashekhar, M.; Choi, Y. C.; Chae, S.; Koley, G.; Spencer,
5
6
7 M. G. Fabrication and Characterization of Pre-Aligned Gallium Nitride Nanowire
8
9
10 Field-Effect Transistors. *Nanotechnology* **2006**, *17*(5), 1264–1271.
11
12
13
14
15 (13) Wu, H.; Cha, H. Y.; Chandrashekhar, M.; Spencer, M. G.; Koley, G. High-Yield GaN
16
17
18 Nanowire Synthesis and Field-Effect Transistor Fabrication. *J. Electron. Mater.*
19
20
21
22 **2006**, *35*(4), 670–674.
23
24
25
26 (14) Yeh, P. C.; Hwa, M. C.; Yu, J. W.; Wu, H. M.; Tsai, H. L.; Lai, C. M.; Huang, J. J.;
27
28
29
30 Yang, J. R.; Peng, L. H. Photon-Assisted Tunneling in GaN Nanowire White Light
31
32
33
34 Emitting Diodes. *Phys. Status Solidi Curr. Top. Solid State Phys.* **2009**, *6*(SUPPL.
35
36
37 **2**), 538–540.
38
39
40
41 (15) Gradečak, S.; Qian, F.; Li, Y.; Park, H. G.; Lieber, C. M. GaN Nanowire Lasers with
42
43
44
45 Low Lasing Thresholds. *Appl. Phys. Lett.* **2005**, *87*(17), 1–3.
46
47
48
49 (16) Sun, J.; Han, M.; Gu, Y.; Yang, Z. xing; Zeng, H. Recent Advances in Group III–V
50
51
52
53 Nanowire Infrared Detectors. *Adv. Opt. Mater.* **2018**, *6*(18), 1–17.
54
55
56
57
58
59
60

- 1
2
3
4 (17) Ryu, S. W.; Zhang, Y.; Leung, B.; Yerino, C.; Han, J. Improved
5
6
7 Photoelectrochemical Water Splitting Efficiency of Nanoporous GaN Photoanode.
8
9
10
11 *Semicond. Sci. Technol.* **2012**, *27*(1), 015014.
12
13
14
15 (18) Park, J.; Mandal, A.; Kang, S.; Chatterjee, U.; Kim, J. S. Hydrogen Generation
16
17
18 Using Non- Polar Coaxial InGaN/GaN Multiple Quantum Well Structure Formed on
19
20
21
22 Hollow n-GaN Nanowires. *Sci. Rep.* **2016**, *6*, 31996.
23
24
25
26 (19) Zhang, L.; Wang, S.; Shao, Y.; Wu, Y.; Sun, C.; Huo, Q.; Zhang, B.; Hu, H.; Hao,
27
28
29 X. One-Step Fabrication of Porous GaN Crystal Membrane and Its Application in
30
31
32
33 Energy Storage. *Sci. Rep.* **2017**, *7*, 1–9.
34
35
36
37
38 (20) Henneghien, A.-L.; Tourbot, G.; Daudin, B.; Lartigue, O.; Désières, Y.; Gérard, J.-
39
40
41 M. Optical Anisotropy and Light Extraction Efficiency of MBE Grown GaN
42
43
44
45 Nanowires Epilayers. *Opt. Express* **2011**, *19*(2), 527.
46
47
48
49 (21) Gurwitz, R.; Shalish, I. Method for Electrical Characterization of Nanowires.
50
51
52
53 *Nanotechnology* **2011**, *22*(43), 435705.
54
55
56
57
58
59
60

- 1
2
3
4 (22) Motayed, A.; Vaudin, M.; Davydov, A. V.; Melngailis, J.; He, M.; Mohammad, S. N.
5
6
7 Diameter Dependent Transport Properties of Gallium Nitride Nanowire Field Effect
8
9
10 Transistors. *Appl. Phys. Lett.* **2007**, *90* (4), 15–18.
11
12
13
14
15 (23) Storm, K.; Halvardsson, F.; Heurlin, M.; Lindgren, D.; Gustafsson, A.; Wu, P. M.;
16
17
18 Monemar, B.; Samuelson, L. Spatially Resolved Hall Effect Measurement in a
19
20
21 Single Semiconductor Nanowire. *Nat. Nanotechnol.* **2012**, *7* (11), 718–722.
22
23
24
25
26 (24) Huang, Y.; Duan, X.; Cui, Y.; Lieber, C. M. Gallium Nitride Nanowire Nanodevices.
27
28
29
30 *Nano Lett.* **2002**, *2* (2), 101–104.
31
32
33
34 (25) Hultin, O.; Otnes, G.; Borgström, M. T.; Björk, M.; Samuelson, L.; Storm, K.
35
36
37
38 Comparing Hall Effect and Field Effect Measurements on the Same Single
39
40
41 Nanowire. *Nano Lett.* **2016**, *16* (1), 205–211.
42
43
44
45 (26) Roddaro, S.; Nilsson, K.; Astromskas, G.; Samuelson, L.; Wernersson, L. E.;
46
47
48
49 Karlström, O.; Wacker, A. InAs Nanowire Metal-Oxide-Semiconductor Capacitors.
50
51
52
53 *Appl. Phys. Lett.* **2008**, *92* (25), 253509.
54
55
56
57
58
59
60

- 1
2
3
4 (27) Chen, Z. H.; Tang, Y. B.; Liu, Y.; Yuan, G. D.; Zhang, W. F.; Zapien, J. A.; Bello, I.;
5
6
7 Zhang, W. J.; Lee, C. S.; Lee, S. T. ZnO Nanowire Arrays Grown on Al:ZnO Buffer
8
9
10 Layers and Their Enhanced Electron Field Emission. *J. Appl. Phys.* **2009**, *106* (6),
11
12
13
14 0–6.
15
16
17
18 (28) Wen, X.; Wu, W.; Ding, Y.; Wang, Z. L. Seedless Synthesis of Patterned ZnO
19
20
21
22 Nanowire Arrays on Metal Thin Films (Au, Ag, Cu, Sn) and Their Application for
23
24
25 Flexible Electromechanical Sensing. *J. Mater. Chem.* **2012**, *22* (19), 9469–9476.
26
27
28
29
30 (29) Parkinson, P.; Dodson, C.; Joyce, H. J.; Bertness, K. A.; Sanford, N. A.; Herz, L.
31
32
33 M.; Johnston, M. B. Noncontact Measurement of Charge Carrier Lifetime and
34
35
36
37 Mobility in GaN Nanowires. *Nano Lett.* **2012**, *12* (9), 4600–4604.
38
39
40
41 (30) Zangoie, S.; Woollam, J. A. Ellipsometric Characterization of Thin Porous GaAs
42
43
44
45 Layers. *J. Mater. Sci. Lett.* **2000**, 2171–2173.
46
47
48
49 (31) Adachi, S. *Optical Constants of Crystalline and Amorphous Semiconductors*;
50
51
52
53 Springer Science: Boston, MA, 1999.
54
55
56
57
58
59
60

- 1
2
3
4 (32) Jones, S. B.; Friedman, S. P. Particle Shape Effects on the Effective Permittivity of
5
6 Anisotropic or Isotropic Media Consisting of Aligned or Randomly Oriented
7
8 Ellipsoidal Particles. *Water Resour. Res.* **2000**, *36* (10), 2821–2833.
9
10
11
12
13
14
15 (33) Kaminska, K.; Amassian, A.; Martinu, L.; Robbie, K. Growth of Vacuum Evaporated
16
17 Ultraporous Silicon Studied with Spectroscopic Ellipsometry and Scanning Electron
18
19 Microscopy. *J. Appl. Phys.* **2005**, *97* (1), 013511.
20
21
22
23
24
25
26 (34) Jellison, G. E.; Modine, F. A. Parameterization of the Optical Functions of
27
28 Amorphous Materials in the Interband Region. *Appl. Phys. Lett.* **1996**, *69* (3), 371–
29
30 373.
31
32
33
34
35
36
37
38 (35) Fujiwara, H.; Kondo, M. Effects of Carrier Concentration on the Dielectric Function
39
40 of ZnO:Ga and In₂O₃:Sn Studied by Spectroscopic Ellipsometry: Analysis of Free-
41
42 Carrier and Band-Edge Absorption. *Phys. Rev. B - Condens. Matter Mater. Phys.*
43
44 **2005**, *71* (7), 1–10.
45
46
47
48
49
50
51
52
53 (36) Drechsler, M.; Hofmann, D. M.; Meyer, B. K.; Detchprohm, T.; Amano, H.; Akasaki,
54
55
56
57
58
59
60

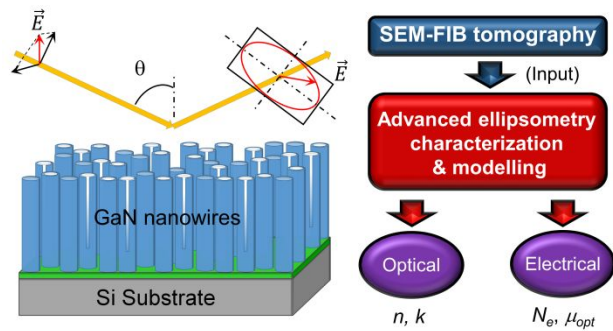
- 1
2
3
4 I. Determination of the Conduction Band Electron Effective Mass in Hexagonal GaN.
5
6
7 *Jpn. J. Appl. Phys.* **1995**, *34* (9), L1177–L1179.
8
9
10
11 (37) Fujiwara, H. *Spectroscopic Ellipsometry: Principles and Applications*; John Wiley &
12
13
14
15 Sons Inc: Chichester, 2007.
16
17
18
19 (38) Chang, C. Y.; Chi, G. C.; Wang, W. M.; Chen, L. I. C.; Chen, K. H.; Ren, F.; Pearton,
20
21
22
23 S. J. Electrical Transport Properties of Single GaN and InN Nanowires. *J. Electron.*
24
25
26 *Mater.* **2006**, *35* (4), 738–743.
27
28
29
30
31 (39) Hilsum, C. Simple Empirical Relationship between Mobility and Carrier
32
33
34 Concentration. *Electron. Lett.* **1974**, *10* (13), 259–260.
35
36
37
38
39 (40) Benner, O.; Blumberg, C.; Arzi, K.; Poloczek, A.; Prost, W.; Tegude, F. J. Electrical
40
41
42 Characterization and Transport Model of N-Gallium Nitride Nanowires. *Appl. Phys.*
43
44
45 *Lett.* **2015**, *107* (8), 1–5.
46
47
48
49
50 (41) Orton, J. W.; Powell, M. J. The Hall Effect in Polycrystalline and Powdered
51
52
53
54 Semiconductors. *Reports Prog. Phys.* **1980**, *43* (11), 1263–1307.
55
56
57
58
59
60

- 1
2
3
4 (42) Xie, Z.; Sui, Y.; Buckeridge, J.; Sokol, A. A.; Keal, T. W.; Walsh, A. Prediction of
5
6
7 Multiband Luminescence Due to the Gallium Vacancy-Oxygen Defect Complex in
8
9
10 GaN. *Appl. Phys. Lett.* **2018**, *112*(26), 1–16.
11
12
13
14
15 (43) Seifert, W.; Franzheld, R.; Butter, E.; Sobotta, H.; Riede, V. On the Origin of Free
16
17
18 Carriers in High-conducting N-GaN. *Cryst. Res. Technol.* **1983**, *18*(3), 383–390.
19
20
21
22
23 (44) Kumar, M.; Poulouse, A. C.; Nakajima, Y.; Sakthikumar, D.; Kumar, V.; Singh, R.
24
25
26 Anomalous Emission from Oxygen Incorporated GaN Nanowires. *Phys. E Low-*
27
28
29 *Dimensional Syst. Nanostructures* **2018**, *104*, 187–191.
30
31
32
33
34 (45) Slack, G. A.; Schowalter, L. J.; Morelli, D.; Freitas, J. A. Some Effects of Oxygen
35
36
37 Impurities on AlN and GaN. *J. Cryst. Growth* **2002**, *246*(3–4), 287–298.
38
39
40
41
42 (46) Feenstra, R. M.; Wood, C. E. C. *Porous Silicon Carbide and Gallium Nitride*; John
43
44
45 Wiley & Sons Inc: Chichester, 2008.
46
47
48
49
50 (47) Shalish, I.; Temkin, H.; Narayanamurti, V. Size-Dependent Surface Luminescence
51
52
53
54 in ZnO Nanowires. *Phys. Rev. B - Condens. Matter Mater. Phys.* **2004**, *69*(24),
55
56
57
58
59
60

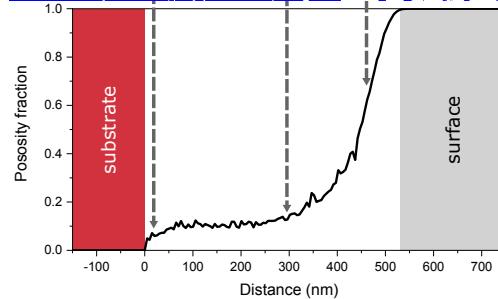
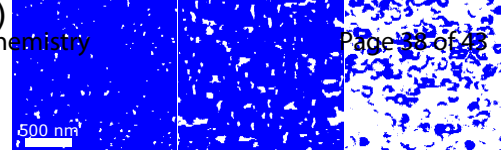
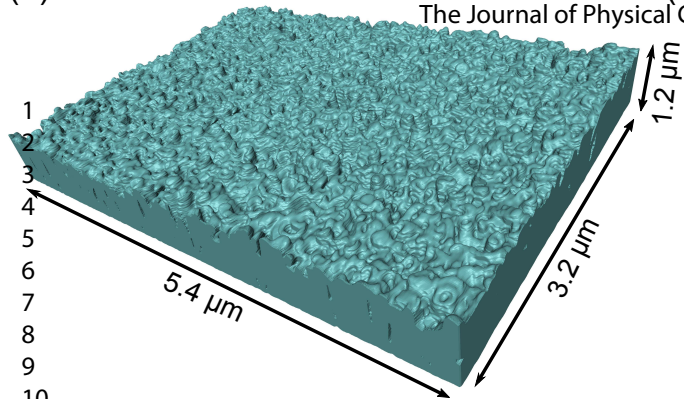
- 1
2
3
4 1–4.
5
6
7
8 (48) Watkins, N. J.; Wicks, G. W.; Gao, Y. Oxidation Study of GaN Using X-Ray
9
10
11 Photoemission Spectroscopy. *Appl. Phys. Lett.* **1999**, *75* (17), 2602–2604.
12
13
14
15
16 (49) Pearton, S. J.; Cho, H.; LaRoche, J. R.; Ren, F.; Wilson, R. G.; Lee, J. W. Oxygen
17
18
19 Diffusion into SiO₂-Capped GaN during Annealing. *Appl. Phys. Lett.* **1999**, *75* (19),
20
21
22
23 2939–2941.
24
25
26
27 (50) Jakiela, R.; Dumiszewska, E.; Caban, P.; Stonert, A.; Turos, A.; Barcz, A. Oxygen
28
29
30
31 Diffusion into GaN from Oxygen Implanted GaN or Al₂O₃. *Phys. Status Solidi Curr.*
32
33
34
35 *Top. Solid State Phys.* **2011**, *8* (5), 1513–1515.
36
37
38
39 (51) Santos, A. J.; Lacroix, B.; Maudet, F.; Corvisier, A.; Paumier, F.; Dupeyrat, C.;
40
41
42 Girardeau, T.; García, R.; Morales, F. M. Surface Oxidation of Amorphous Si and
43
44
45
46 Ge Slanted Columnar and Mesoporous Thin Films: Evidence, Scrutiny and
47
48
49 Limitations for Infrared Optics. *Appl. Surf. Sci.* **2019**, *493*, 807–817.
50
51
52
53
54
55
56
57
58
59
60

1
2
3
4
5
6
7
8
9
10
11
12
13
14
15
16
17
18
19
20
21
22
23
24
25
26
27
28
29
30
31
32
33
34
35
36
37
38
39
40
41
42
43
44
45
46
47
48
49
50
51
52
53
54
55
56
57
58
59
60

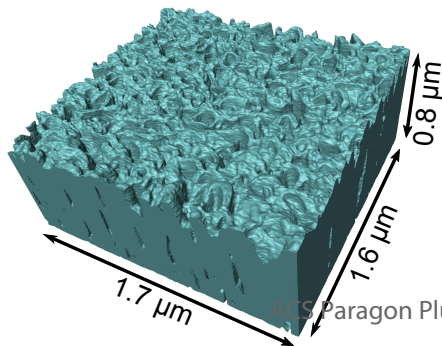
TOC GRAPHIC



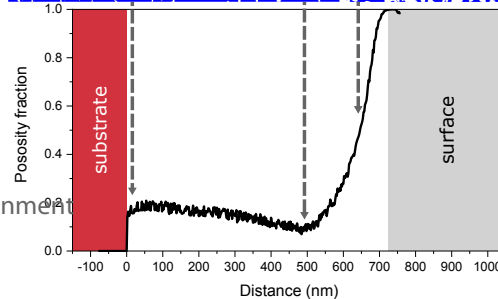
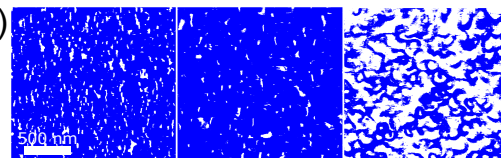
(a)

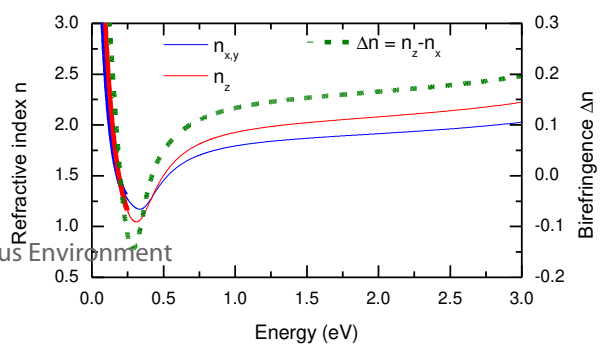
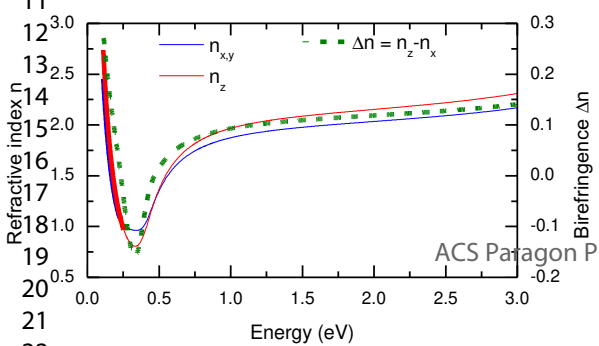
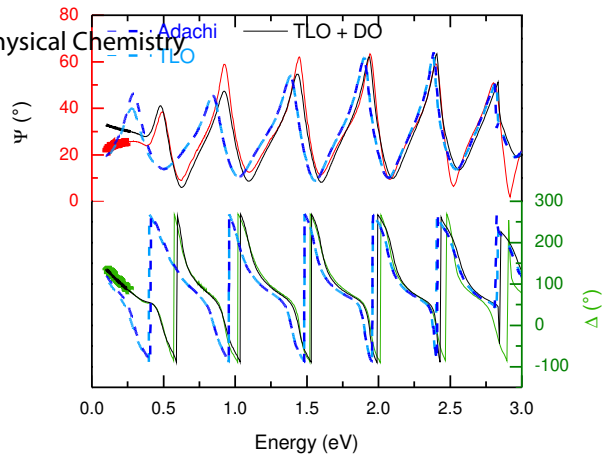
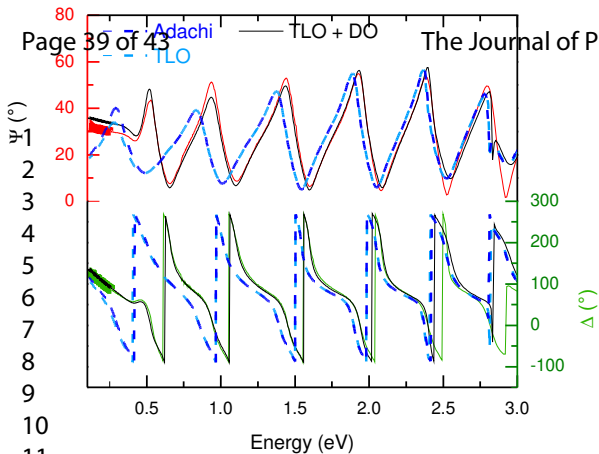


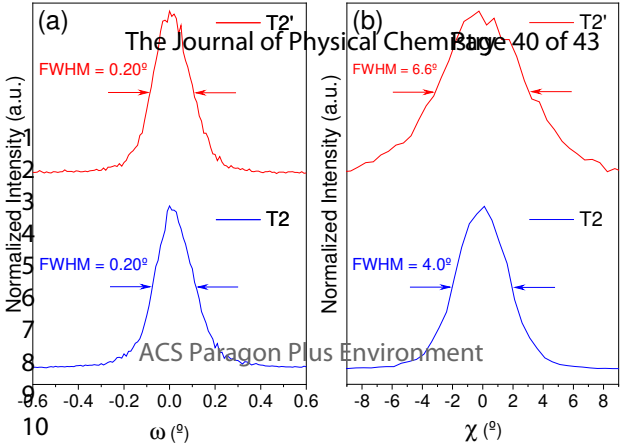
(b)

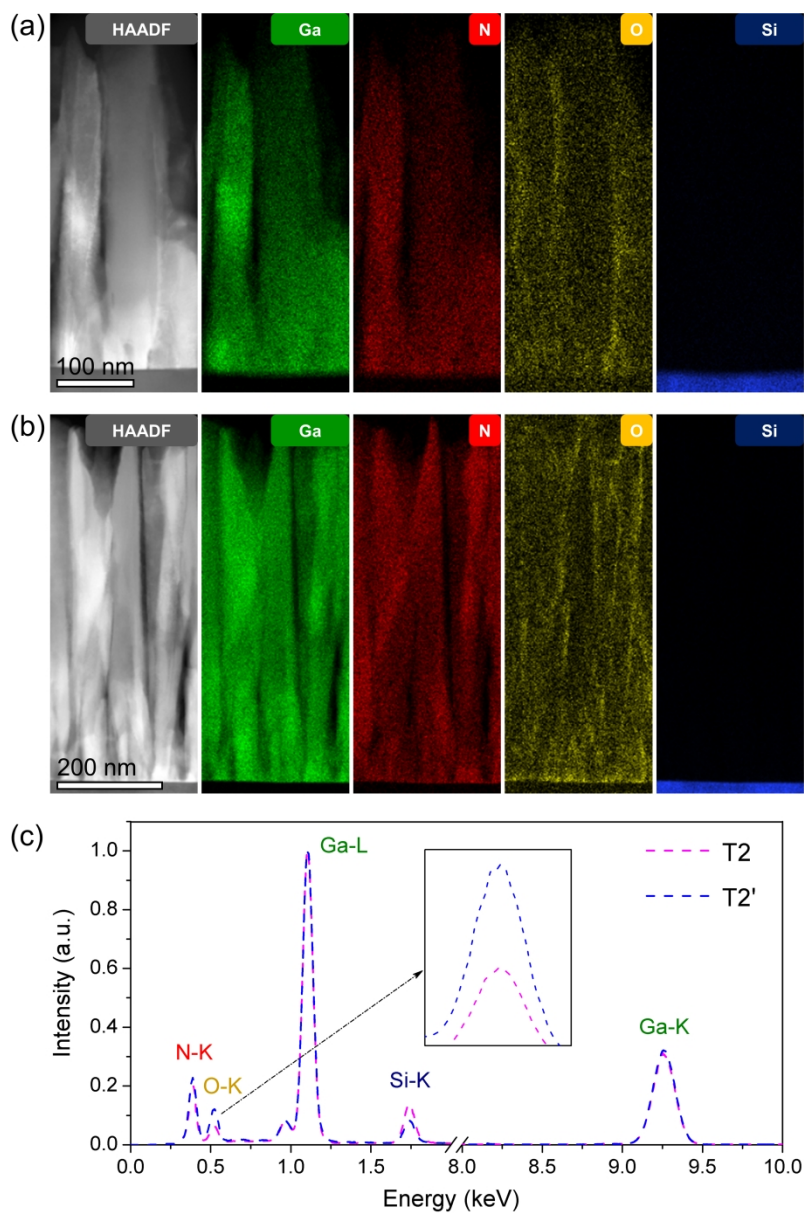


(d)



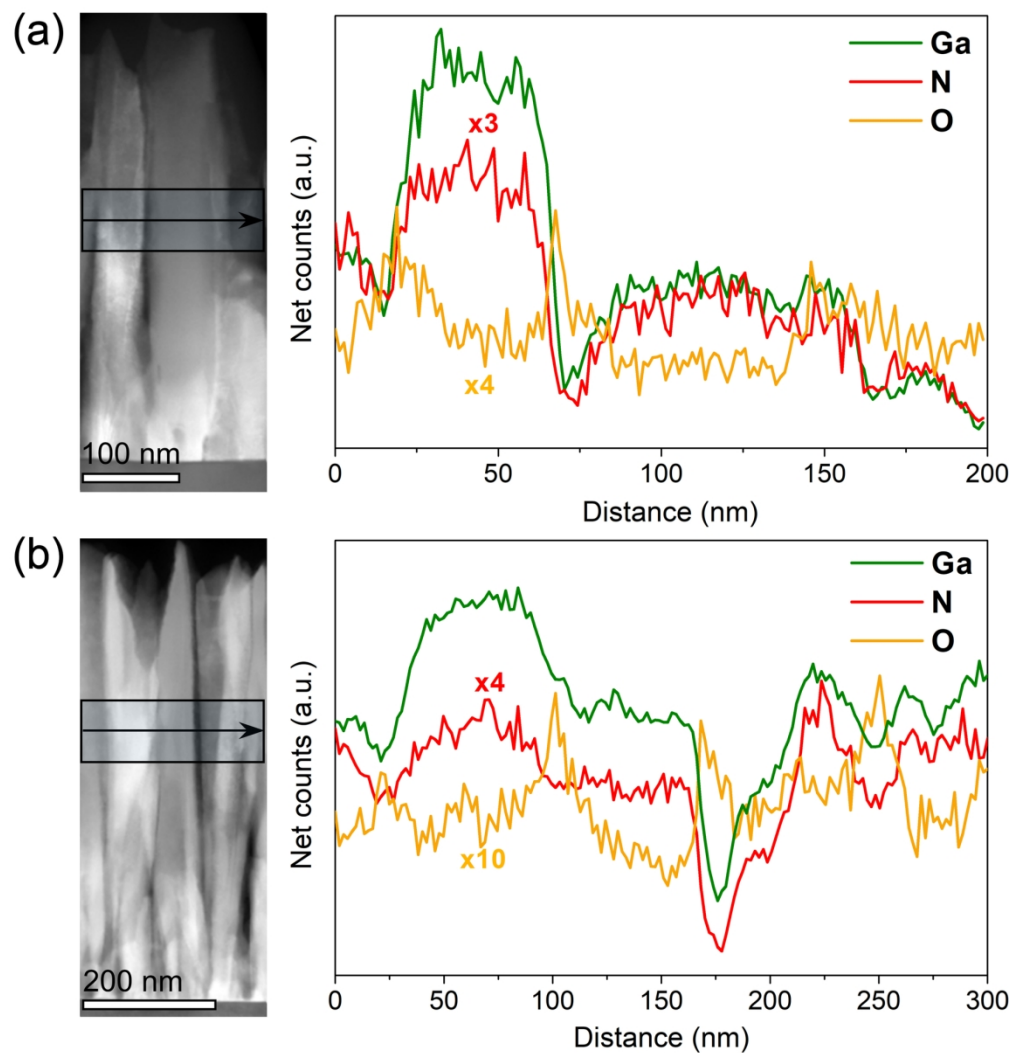






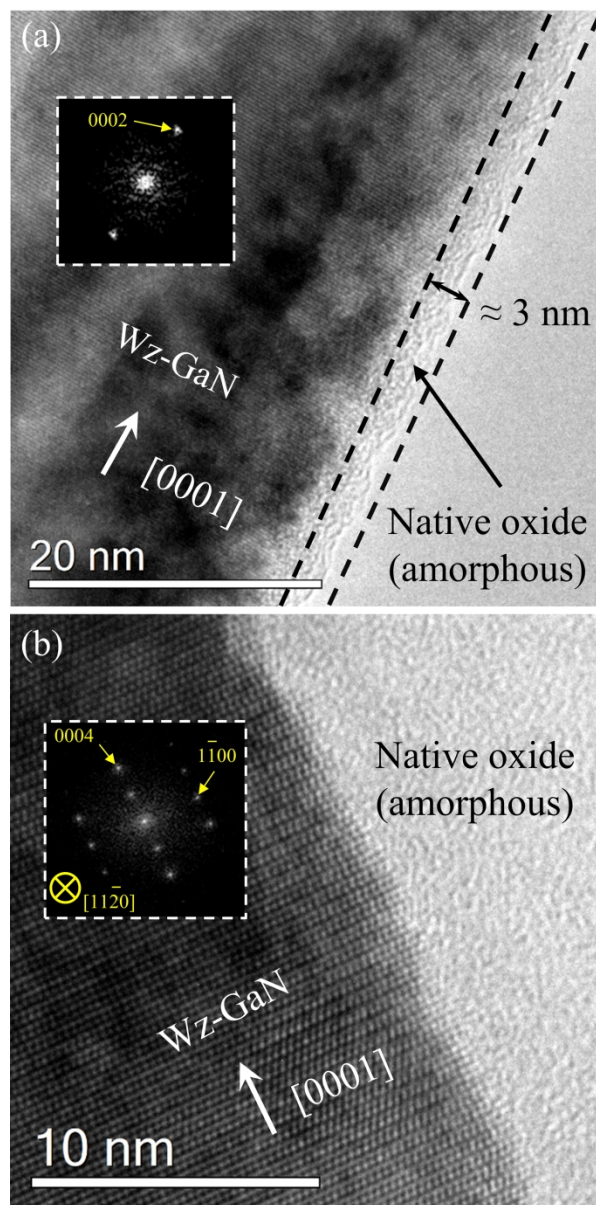
45 STEM-HAADF and EDX elemental maps of (a) T2 and (b) T2' samples obtained for Ga, N, O and Si atoms.
46 (c) EDX spectra, normalized at Ga-L α peak (1098 eV), for T2 (magenta dashed line) and T2' (blue dashed
47 line) samples. The inset corresponds to the feature of the O-K α peak (525 eV).
48

49 82x123mm (1000 x 1000 DPI)



41 STEM-HAADF and Ga, N and O EDX elemental profiles for (a) T2 and (b) T2' samples. Note that such profiles
42 were integrated across the NWs following the direction indicated by the arrows.

43 81x88mm (600 x 600 DPI)



High-resolution TEM micrographs and corresponding FFT diffractions of single nanowires of (a) T2 and (b) T2' samples. Note that these TEM observations were conducted on two FIB lamellae prepared by using the same SEM-FIB systems as for FIB tomography experiments.

79x162mm (600 x 600 DPI)